Article:
Zhang, J, Xie, F, Tian, W et al. (7 more authors) (2017) Influence of the Arctic Oscillation on the Vertical Distribution of Wintertime Ozone in the Stratosphere and Upper Troposphere over Northern Hemisphere. Journal of Climate, 30 (8). pp. 2905-2919. ISSN 0894-8755

https://doi.org/10.1175/JCLI-D-16-0651.1

Influence of the Arctic Oscillation on the Vertical Distribution of Wintertime Ozone in the Stratosphere and Upper Troposphere over the Northern Hemisphere

JIANKAI ZHANG,[a] FEI XIE,[b] WENSHOU TIAN,[a] YUANYUAN HAN,[a] KEQUAN ZHANG,[a] YULEI QI,[c] MARTYN CHIPPERFIELD,[d] WUHU FENG,[d,e] JINLONG HUANG,[a] AND JIANCHUAN SHU[f]

[a] *Key Laboratory for Semi-Arid Climate Change of the Ministry of Education, College of Atmospheric Sciences, Lanzhou University, Lanzhou, China*
[b] *State Key Laboratory of Earth Surface Processes and Resource Ecology, College of Global Change and Earth System Science, Beijing Normal University, Beijing, China*
[c] *School of Atmospheric Sciences, Chengdu University of Information Technology, Chengdu, China*
[d] *National Center for Atmospheric Science, School of Earth and Environment, University of Leeds, Leeds, United Kingdom*
[e] *School of Chemistry, University of Leeds, Leeds, United Kingdom*
[f] *Institute of Plateau Meteorology, China Meteorological Administration, Chengdu, China*

(Manuscript received 30 August 2016, in final form 28 December 2016)

ABSTRACT

The influence of the Arctic Oscillation (AO) on the vertical distribution of stratospheric ozone in the Northern Hemisphere in winter is analyzed using observations and an offline chemical transport model. Positive ozone anomalies are found at low latitudes (0°–30°N) and there are three negative anomaly centers in the northern mid- and high latitudes during positive AO phases. The negative anomalies are located in the Arctic middle stratosphere (~30 hPa; 70°–90°N), Arctic upper troposphere–lower stratosphere (UTLS; 150–300 hPa, 70°–90°N), and midlatitude UTLS (70–300 hPa, 30°–60°N). Further analysis shows that anomalous dynamical transport related to AO variability primarily controls these ozone changes. During positive AO events, positive ozone anomalies between 0° and 30°N at 50–150 hPa are related to the weakened meridional transport of the Brewer–Dobson circulation (BDC) and enhanced eddy transport. The negative ozone anomalies in the Arctic middle stratosphere are also caused by the weakened BDC, while the negative ozone anomalies in the Arctic UTLS are caused by the increased tropopause height, weakened BDC vertical transport, weaker exchange between the midlatitudes and the Arctic, and enhanced ozone depletion via heterogeneous chemistry. The negative ozone anomalies in the midlatitude UTLS are mainly due to enhanced eddy transport from the midlatitudes to the latitudes equatorward of 30°N, while the transport of ozone-poor air from the Arctic to the midlatitudes makes a minor contribution. Interpreting AO-related variability of stratospheric ozone, especially in the UTLS, would be helpful for the prediction of tropospheric ozone variability caused by the AO.

1. Introduction

Atmospheric ozone plays an important role in modulating the radiative budget of climate system (e.g., Thompson et al. 2011; Li et al. 2016; Xie et al. 2016) and protecting life on Earth from harmful solar ultraviolet radiation (e.g., Kerr and McElroy 1993). However, interpretation of long-term ozone variation is difficult since the ozone field exhibits not only a complicated trend, forced by changes in ozone-depleting substances superimposed on a changing climate, but also interannual variability related to various meteorological conditions (e.g., Weiss et al. 2001; Hadjinicolaou et al. 2002; Tian and Chipperfield 2005; Austin et al. 2010; Eyring et al. 2010; Liu et al. 2013; Douglass et al. 2014). The World Meteorological Organization (WMO 2007, 2011) highlighted the fact that meteorology can also significantly influence the long-term trend of total ozone column (TOC); in particular, meteorological variability can explain as much as 20%–50% of TOC variability in the extratropics of the Northern Hemisphere during winter and spring. Therefore, separating the different sources of ozone variability is crucial for understanding the global ozone response to varying anthropogenic emissions and climate change (e.g., Austin and Wilson 2006; Hess and Lamarque 2007; Li et al. 2009; Frossard et al. 2013; Rieder et al. 2013). Numerous previous studies have analyzed the stratospheric ozone variability

Corresponding author e-mail: Dr. Fei Xie, xiefei@bnu.edu.cn

DOI: 10.1175/JCLI-D-16-0651.1

caused by external processes such as the solar cycle (e.g., Chandra and McPeters 1994; Rozanov et al. 2005; Dhomse et al. 2006) and volcanic aerosols (e.g., Hofmann and Oltmans 1993; Solomon et al. 1996; Rozanov et al. 2002; Dhomse et al. 2015), which can induce considerable variation in ozone over both short and long periods. TOC variations can also be caused by changes in the surface climate (Zhang et al. 2014). Other studies have reported the effects of internal climate variability on ozone, including phenomena such as the Madden–Julian oscillation (e.g., Fujiwara et al. 1998; Tian et al. 2007; C. Liu et al. 2009; Weare 2010; Li et al. 2012; Y. Zhang et al. 2015), El Niño–Southern Oscillation (ENSO) (e.g., Ziemke and Chandra 1999; Cagnazzo et al. 2009; Randel et al. 2009; Xie et al. 2014a,b; J. Zhang et al. 2015a,b), the quasi-biennial oscillation (e.g., Angell and Korshover 1973; Bowman 1989; Tung and Yang 1994; Dhomse 2006; Li and Tung 2014), and the Arctic Oscillation (AO) or North Atlantic Oscillation (NAO) (e.g., Appenzeller et al. 2000; Schnadt and Dameris 2003; Lamarque and Hess 2004; Creilson et al. 2005; Steinbrecht et al. 2011). In fact, quantification of this internally driven ozone variability forms a key part of the assessment of the performance of chemistry–climate models (CCMs). Cagnazzo et al. (2009) noted that the spread in the ENSO signal in stratospheric ozone in the winter Northern Hemisphere modeled by CCMs is closely related to the large stratospheric internal variability that is dependent essentially on the simulation of ENSO teleconnections in the troposphere.

The AO is the dominant mode of internal climate variability in the Northern Hemisphere and is an indication of varying interaction between the mid-to-high latitudes and the Arctic, in both atmospheric mass and circulation (Thompson and Wallace 2000; Thompson and Wallace 2001). Most previous studies of AO-related ozone variability have focused on the influence of the AO on tropospheric ozone, presumably because understanding the natural variability of tropospheric ozone is useful for forecasting air pollution events (Lamarque and Hess 2004; Creilson et al. 2005; Hess and Lamarque 2007; J. Liu et al. 2009; Liu et al. 2011). These analyses confirmed that AO variability can exert a significant influence on ozone. Hess and Lamarque (2007) pointed out that the AO can modulate tropospheric ozone concentrations by up to 5 ppbv during February and March. Lamarque and Hess (2004) found that AO variability can account for as much as 50% of the ozone variability in the lower troposphere over North America in spring. Although the AO pattern shows strong zonal symmetry, the AO-related ozone variability pattern features considerable regional structure. An analysis of Creilson et al. (2005) showed that there is a statistically significant correlation between the AO and tropospheric ozone variations over the North Atlantic during spring, whereas there is no equivalent correlation over the Pacific Ocean. The zonally asymmetric AO-driven response may depend on the relative contributions of stratosphere–troposphere exchange (STE), which is directly affected by the AO (Lamarque and Hess 2004), and anthropogenic emissions to tropospheric ozone in different regions. It is known that modulations in STE dominate the tropospheric ozone variability associated with the AO over northern Canada, northeastern Asia, and the Arctic (Hess and Lamarque 2007). Therefore, better understanding of the influence of the AO on stratospheric ozone is critical to the assessment of AO-related ozone variability in the troposphere.

Using satellite data, Steinbrecht et al. (2011) found that the TOC in 2010 over Hohenpeissenberg (48°N, 11°E) was the largest for the two past decades. Their analysis found that the large ozone anomalies in 2010 were related to meteorological variability and, in particular, to the unusually persistent negative phase of the AO. They also estimated that the AO index can account for approximately 8 Dobson units (DU) of TOC increase over Hohenpeissenberg in 2010. Weiss et al. (2001) suggested that the AO has a nonnegligible impact that can modulate TOC variations in the mid- and high latitudes. Most studies have linked the AO-related variability in the TOC to changes in tropopause height associated with the AO pattern (Appenzeller et al. 2000; Weiss et al. 2001). In addition, previous studies (e.g., Schnadt and Dameris 2003; Reinsel et al. 2005; Steinbrecht et al. 2011) have noted that there is a significant AO signal in the TOC that is manifested mainly in stratospheric ozone. This implies a strong effect of the AO on the stratospheric ozone distribution. However, the details regarding the vertical and meridional structures of AO-related stratospheric ozone variation have attracted less attention. The altitude at which the largest AO-related ozone response occurs can, in fact, give an indication of whether dynamical or chemical processes dominate AO-related ozone variability. Generally speaking, if the largest ozone variability associated with the AO occurs in the lower stratosphere, it is likely to be mainly related to dynamical processes, while chemical processes dominate upper stratospheric ozone changes (Solomon et al. 1985; Allen et al. 2012).

It has been reported that the Arctic polar vortex has weakened during the 2000s compared with the 1980s (Alexeev et al. 2012; Zhang et al. 2016) with a trend that might be related to "Arctic amplification" (Cohen et al. 2014). These processes are also consistent with the decrease in the AO since the late 1980s (Overland and Wang 2005; Cohen et al. 2012). In fact, AO variability is essentially an indication of changes in the polar vortex; that is, a

strengthened (weakened) polar vortex corresponds to the positive (negative) AO phase (Baldwin and Dunkerton 2001). During the positive AO phase, the vortex cools dramatically and increased regions of polar stratospheric clouds form in its interior, leading to large Arctic ozone depletion (Manney et al. 2011). Vortex air with low ozone concentrations can be transported into the midlatitudes through the formation of filaments (Orsolini et al. 1995; Knudsen and Grooss 2000). During the negative AO phase, the vortex is weakened and ozone-poor air in the Arctic is more easily transported to the mid-to-high latitudes, leading to decreases in ozone concentration at those latitudes. Therefore, it is also of interest to investigate the influence of ozone dilution events caused by the Arctic vortex during anomalous AO phases on stratospheric ozone variations in the mid- and high latitudes. The present work explores AO-related stratospheric ozone variations over the Northern Hemisphere and the associated dynamical and chemical processes. The Arctic vortex and AO patterns are strongest in winter, and stratosphere–troposphere interaction is weaker in spring, summer, and fall than in winter (Holton et al. 1995). Therefore, the present study focuses on AO-related stratospheric ozone variability in winter.

The paper is organized as follows. The data, method, and model used are introduced and briefly described in section 2. In section 3, the patterns of ozone variability associated with AO variability are presented. The dynamical and chemical processes responsible for these AO-related ozone variations are analyzed in section 4. Finally, our results and conclusions are summarized in section 5.

2. Data, method, and model

The daily AO index is constructed by projecting the daily 1000-hPa height anomalies poleward of 20°N onto the leading pattern of the AO and then averaging as a monthly mean. (Detailed information about the AO index can be found online at http://www.cpc.ncep.noaa.gov/products/precip/CWlink/daily_ao_index/ao_index.html.) Monthly mean ozone profiles for the period 1979–2015 are taken from the NASA Modern-Era Retrospective Analysis for Research and Applications, version 2 (MERRA-2; Bosilovich et al. 2015; https://disc.sci.gsfc.nasa.gov/daac-bin/FTPSubset.pl?LOOKUPID_List=MAIMCPASM) and used to investigate vertical ozone variability associated with the AO. The MERRA-2 data use 42 pressure levels from the surface to 0.1 hPa. The vertical resolution of MERRA-2 is approximately 1–2 km in the upper troposphere–lower stratosphere and 2–4 km in the middle and upper stratosphere. MERRA-2 is assimilated by the Goddard Earth Observing System Model, version 5 (GEOS-5) with ozone from the Solar Backscatter Ultraviolet (SBUV) radiometers from October 1978 to October 2004, and thereafter from the Ozone Monitoring Instrument (OMI) and *Aura* Microwave Limb Sounder (MLS) (Bosilovich et al. 2015). Previous studies (e.g., Rieder et al. 2014; J. Zhang et al. 2015a) have shown that MERRA-2 ozone data compare well with satellite ozone observations and so can indeed be used to analyze interannual ozone variability. Monthly mean partial column ozone profiles at 21 vertical layers during the period 1979–2014 from the SBUV dataset (version 8.6) are also used. The SBUV instruments infer ozone profiles from backscattered radiance measurements at several different ultraviolet wavelengths. The pressure at the bottom of the SBUV layer L ranging from 1 to 21 is $1013.25 \times 10^{-(L-1)/5}$ hPa, and each layer is about 3.2 km thick (Bhartia et al. 2013). The resolution in the lower stratosphere and troposphere is 10–15 km. More details about this dataset can be found in McPeters et al. (2013) and Frith et al. (2014). Because of the poor vertical resolution of SBUV data, ozone measurement from the MLS satellite instrument is used for comparison. The MLS data used here are obtained from MLS version 3.3 level-2 products. Ozone (O_3) profiles are available at 12 levels ranging from 261 to 0.02 hPa. The vertical resolution for the standard MLS O_3 product is approximately 2.5–3 km in the uppermost troposphere and lower stratosphere. We processed individual profiles following the instructions of "data screening" in Livesey et al. (2011). The typical single-profile precisions for ozone are 0.03 ppmv at 150 hPa and 0.1 ppmv at 10 hPa (Livesey et al. 2011). We constructed gridded monthly data by averaging profiles inside bins with resolution of 5° latitude × 10° longitude. MLS ozone data used here cover 2004–15.

Brewer–Dobson circulation (BDC) and eddy transports are calculated using terms (1) and (2), respectively (Monier and Weare 2011; Abalos et al. 2013):

$$\frac{\partial \overline{\chi_{O_3}}}{\partial t} = \frac{\overline{v}^*}{R}\frac{\partial \overline{\chi_{O_3}}}{\partial \phi} - \overline{w}^*\frac{\partial \overline{\chi_{O_3}}}{\partial z} \tag{1}$$

$$-\frac{1}{\rho_0}\nabla \cdot \mathbf{M} \tag{2}$$

$$+\overline{S}, \tag{3}$$

where $\overline{S}$ is the net chemical ozone production term, $\overline{\chi_{O_3}}$ is zonal-mean ozone concentration, $\overline{v}^*$ and $\overline{w}^*$ are the meridional and vertical BDC velocities (Andrews et al. 1987), $\mathbf{M}$ is the eddy flux vector

$$\left[\rho_0\left(\overline{v'\chi'_{O_3}} - \frac{\overline{v'\theta'}}{\overline{\theta}_z}\frac{\partial \overline{\chi_{O_3}}}{\partial z}\right), \rho_0\left(\overline{w'\chi'_{O_3}} + \frac{1}{R}\frac{\overline{v'\theta'}}{\overline{\theta}_z}\frac{\partial \overline{\chi_{O_3}}}{\partial \phi}\right)\right],$$

$\nabla \cdot \mathbf{M}$ is the divergence of the eddy flux vector and represents the eddy transport of ozone, ρ_0 is air density, θ is potential temperature, R is Earth's radius, t is time, and ϕ and z are latitude and height, respectively.

In the present study, we use the Toulouse Offline Model of Chemistry and Transport (TOMCAT)/Single Layer Isentropic Model of Chemistry and Transport (SLIMCAT) three-dimensional offline chemical transport model (Chipperfield 2006) to analyze the chemical processes involved in AO-related ozone variability. The model uses horizontal winds and temperature from the European Centre for Medium-Range Weather Forecasts (ECMWF) interim reanalysis (ERA-Interim; Dee et al. 2011). Previous studies have found that the wind and temperature fields from ERA-Interim agree well with those from MERRA-2, especially in the mid- and high latitudes (Rienecker et al. 2011; Lindsay et al. 2014). The SLIMCAT model used in this study for long-term simulations (1979–2015) performs with a coarse horizontal resolution of about 5.625° latitude × 5.625° longitude and 32 levels from the surface to 60 km. The model uses a hybrid sigma–pressure (σ–p) vertical coordinate (Chipperfield 2006) with detailed tropospheric and stratospheric chemistry. Vertical advection is calculated from the divergence of the horizontal mass flux (Chipperfield 2006), and chemical tracers are advected, conserving second-order moments (Prather 1986). The SLIMCAT model has been extensively evaluated against various ozone satellite and sounding datasets, and provides a good representation of stratospheric chemistry (e.g., Chipperfield 2006; Feng et al. 2007, 2011). ERA-Interim data to force the SLIMCAT model were available for the period 1979–2015. The SLIMCAT simulation initializes a ''passive odd-oxygen'' tracer that is set equal to the modeled chemical $O_x = O(^3P) + O(^1D) + O_3$ concentration on 1 December every year for the Northern Hemisphere and then advected passively without chemistry. At any point and time after 1 December, the difference between this passive O_x and the model's chemically integrated O_x is the net chemical O_x change in air that has been advected to the point (Feng et al. 2005). O_x is mainly O_3 below 30 km where the concentrations of $O(^3P)$ and $O(^1D)$ are small, especially in winter when there is no sunlight in the polar region. Hereafter, the passive O_x is referred to as dynamical ozone while the chemical O_x change is called chemical ozone. Two types of experiments were performed with the SLIMCAT model: the first one uses full chemistry and the second one employs full chemistry, but without considering all heterogeneous chemical processes. The chemical ozone is further divided into chemical ozone with and without the inclusion of heterogeneous chemistry (HC), referred to as HC ozone and non-HC ozone, respectively.

3. AO-related ozone winter variability

Figure 1a shows the correlation between the AO index and zonal-mean ozone from MERRA-2, as a function of latitude and height over the Northern Hemisphere during winter. It can be seen that the AO and stratospheric ozone are positively correlated in low latitudes, but are generally negatively correlated in the mid- and high latitudes. In particular, there are three distinct areas of negative correlation in the extratropics centered in the midlatitude upper troposphere–lower stratosphere (UTLS) (70–300 hPa, 30°–60°N), the Arctic middle stratosphere (~30 hPa, 70°–90°N), and the Arctic UTLS (300–100 hPa, 70°–90°N). In this study, we use the terms ''midlatitude UTLS,'' ''Arctic middle stratosphere,'' and ''Arctic UTLS'' to represent these three specific regions in order to make expression concise. Similar negative ozone anomalies in the Arctic UTLS during the positive AO phase have been found in previous studies (Lamarque and Hess 2004; Hess and Lamarque 2007). However, the negative correlation coefficients in the midlatitude UTLS and in the Arctic middle stratosphere have not received as much attention. In addition, we find that in the MERRA-2 data the midlatitude UTLS is the only region that shows significant correlations between ozone and the AO in all four seasons (not shown), suggesting that AO variability exerts a particularly strong influence on ozone in this region during winter.

Figures 1b and 1c show similar correlations between the AO and ozone using MLS and SBUV satellite measurements. As in the MERRA-2 data (Fig. 1a), there are positive correlations between the AO and ozone in low latitudes (0°–30°N) and negative correlations in the midlatitude UTLS. Note that the positive correlations exist below the altitude of 150 hPa in the tropics derived from the MERRA-2 data and SBUV observations (Figs. 1a,c), while there are relatively weak negative correlations in this region in the MLS data (Fig. 1b). This discrepancy might be related to the large uncertainties in ozone profile retrieval near the tropical tropopause, due to cloud effects (Degenstein et al. 2009; Sioris et al. 2014). In addition, two centers of negative correlation are found in the Arctic middle stratosphere and Arctic UTLS in the MLS data, which is consistent with MERRA-2. SBUV data are not available in the Arctic due to the absence of solar radiation in the winter polar night. Figure 1d shows the equivalent correlation between the AO and ozone simulated by the SLIMCAT model with full chemistry. As with the reanalysis and satellite data, the SLIMCAT simulation also shows three negative correlation centers in the midlatitude UTLS, the Arctic middle stratosphere, and the Arctic UTLS, as well as the dipole pattern between the tropics and extratropics, further supporting the results from MERRA-2 data. The weak negative correlation coefficients between the AO and ozone below the altitude

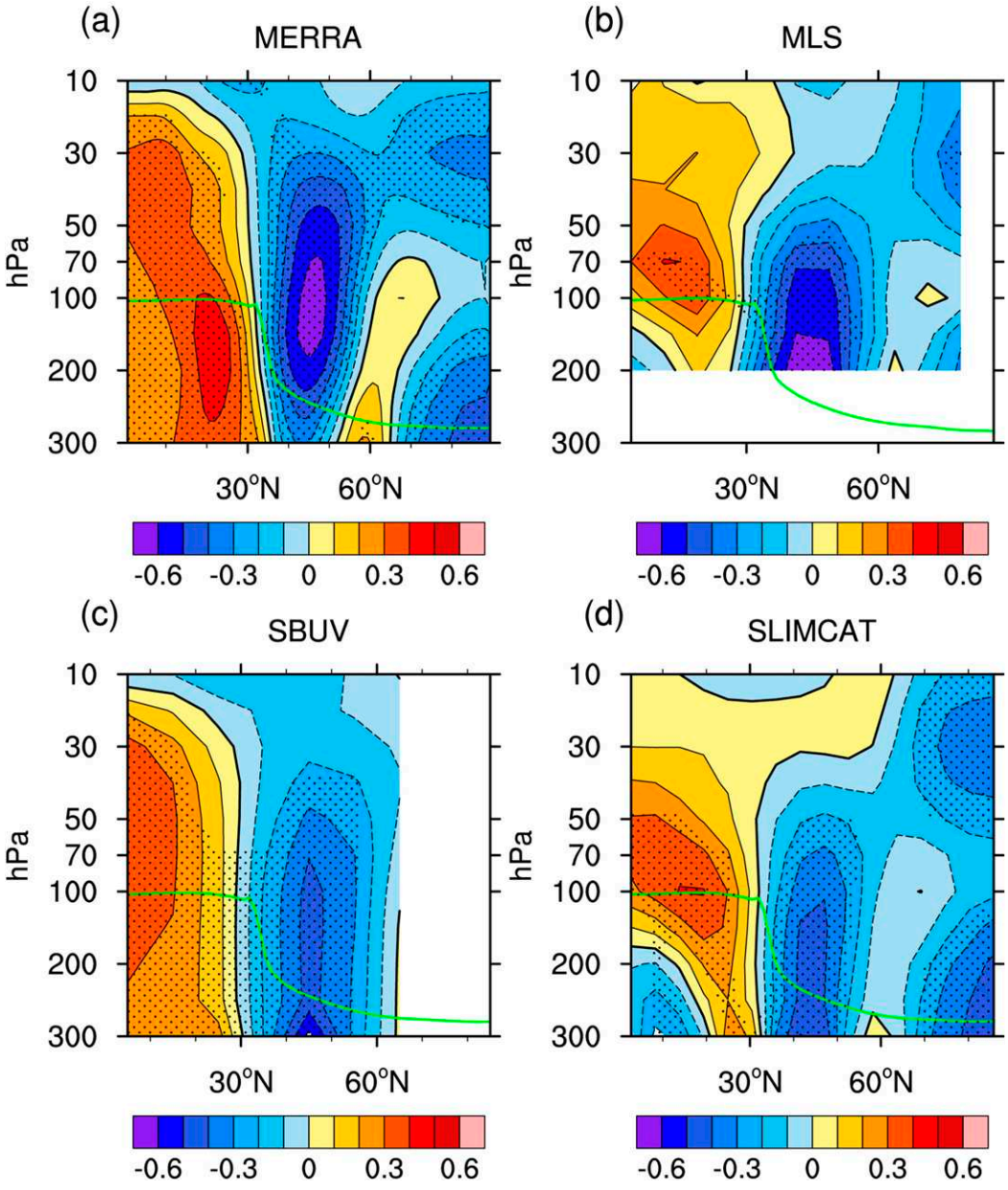

FIG. 1. Correlation coefficients between the AO index and zonal-mean ozone concentration from 300 to 10 hPa over the Northern Hemisphere during winter, for ozone data from (a) MERRA-2, (b) MLS, (c) SBUV, and (d) SLIMCAT. The correlation coefficients over the dotted regions are statistically significant at the 90% confidence level according to the Student's *t* test. No data were available in the white regions in (b) and (c). MLS data cover the period 2004–15, SBUV data are available for the period 1979–2014, and MERRA-2 and SLIMCAT data cover the period 1979–2015. The green line denotes the thermal tropopause height during winter derived from MERRA-2 data.

of 150 hPa in the tropics in SLIMCAT are also consistent with the MLS data. The factors responsible for the positive AO–ozone correlation in the tropics and the three negative correlation centers in the extratropics are discussed in detail in section 4.

To further verify the influence of AO variability on stratospheric and upper tropospheric ozone over the Northern Hemisphere during winter, a composite analysis is performed with respect to the December–February (DJF)-mean AO index. Figure 2 shows the normalized DJF-mean AO index for the period 1979–2015 along with the plus or minus one standard deviation threshold that is used to define strong anomalous AO events. The criterion for strong positive

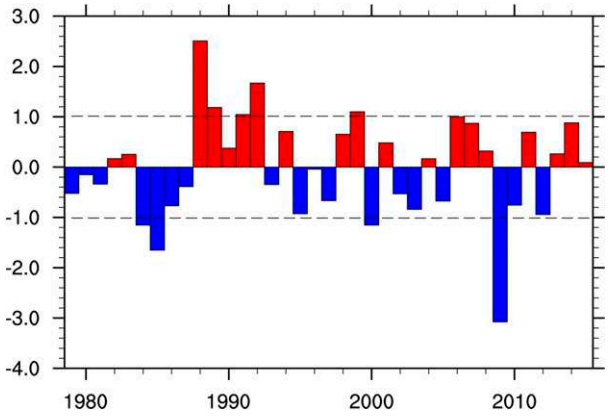

FIG. 2. Time series of the normalized DJF-mean AO index for 1979–2015. The dashed lines mark plus or minus one standard deviation of the time series.

(negative) AO events is that the DJF mean of normalized AO index with respect to the climatology mean from 1979 to 2015 is greater than 1 (less than −1). According to this criterion, the winters of 1988/89, 1989/90, 1991/92, 1992/93, 1999/2000, and 2006/07 are periods of positive AO anomalies, whereas the winters of 1984/85, 1985/86, 2000/01, and 2009/10 correspond to the negative AO phase. Here, the positive (negative) AO composite for a given field is calculated by averaging the field over all winter (i.e., DJF) months during anomalous positive (negative) AO years. The results are not sensitive to a small change in the threshold for anomalous AO events (e.g., using 0.5 or 1.0 standard deviation).

Figures 3a and 3b show the DJF-mean composite ozone anomalies associated with the positive and negative AO phases from MERRA-2 data, respectively. The patterns of ozone anomalies due to AO variability are similar to the patterns of correlation between the AO and ozone; that is, positive (negative) correlation coefficients (Fig. 1) correspond to positive (negative) ozone anomalies (Fig. 3a) during the positive AO phase. This suggests that our extraction of the signal of AO-related variations in ozone over the Northern Hemisphere is reliable. Figure 3c shows the difference in percentage ozone anomalies between the positive and negative AO events. It is seen that the largest differences (∼−30%) occur in the Arctic UTLS, rather than in the midlatitude UTLS (−16%) where the largest negative correlations between the AO index and ozone are located (Fig. 1). This might be related to the stronger ozone variability in the Arctic than in the midlatitudes. Ozone differences in the Arctic middle stratosphere can reach about −20%. Similar results are found using the SLIMCAT output (Figs. 3d–f), although the ozone anomalies associated with AO events are somewhat larger than those in the MERRA-2 data (Figs. 3a–c).

4. Factors responsible for AO-related ozone variability

Figures 4a and 4b show the ozone differences between positive and negative AO events that can be attributed to dynamical and chemical processes, respectively, from the SLIMCAT simulations. Hereafter, we use the term ''dynamical ozone'' to refer to ozone variations caused by dynamical processes, and the term ''chemical ozone'' to refer to variations occurring due to chemical reactions. Dynamical ozone signals account for most of the ozone variations associated with AO variability (Figs. 3c,f and 4a). This indicates that AO-related ozone variability in winter occurs mainly through dynamical mechanisms. In the Arctic, dynamical depletions of ozone are largest in the middle stratosphere and the UTLS, while dynamical transport enhances ozone concentrations between 50 and 150 hPa within 0°–30°N. Chemical ozone depletion is much weaker than dynamical depletion (Fig. 4). The chemistry associated with the positive AO phase depletes ozone in the Arctic middle stratosphere, but enhances ozone at 100 hPa in the tropics and in the Arctic at 10–30 and 250–300 hPa, as discussed below. Interestingly, the chemical and dynamical ozone anomaly patterns show a strong antisymmetry, which means that the two effects partially offset each other during anomalous AO events.

To clarify which chemical processes determine the chemical ozone changes, ozone differences between positive and negative AO phases derived from the experiments with and without heterogeneous chemistry are shown in Fig. 5. It is found that gas-phase chemistry (i.e., without heterogeneous chemical processes) increases chemical ozone in the Arctic middle stratosphere and in the tropics at 100 hPa (Fig. 5a). In contrast, there exists chemical ozone loss between 50 and 30 hPa in the tropics caused by gas-phase chemistry. The positive ozone anomalies due to gas-phase chemistry in the Arctic middle stratosphere are caused by slower reaction rates of ozone loss associated with cooling temperature (Fig. 5b) and vice versa for the negative ozone anomalies between 50 and 30 hPa in the tropics. When the heterogeneous chemistry is included in the model, there is significantly enhanced chemical ozone loss in the Arctic between 30 and 200 hPa during winter, suggesting that the chemical ozone loss due to increased active chlorine and bromine in heterogeneously chemical processes makes a large contribution to the total chemical ozone loss in these pressure layers (Figs. 5c and 4b). The strengthening of heterogeneous reactions is

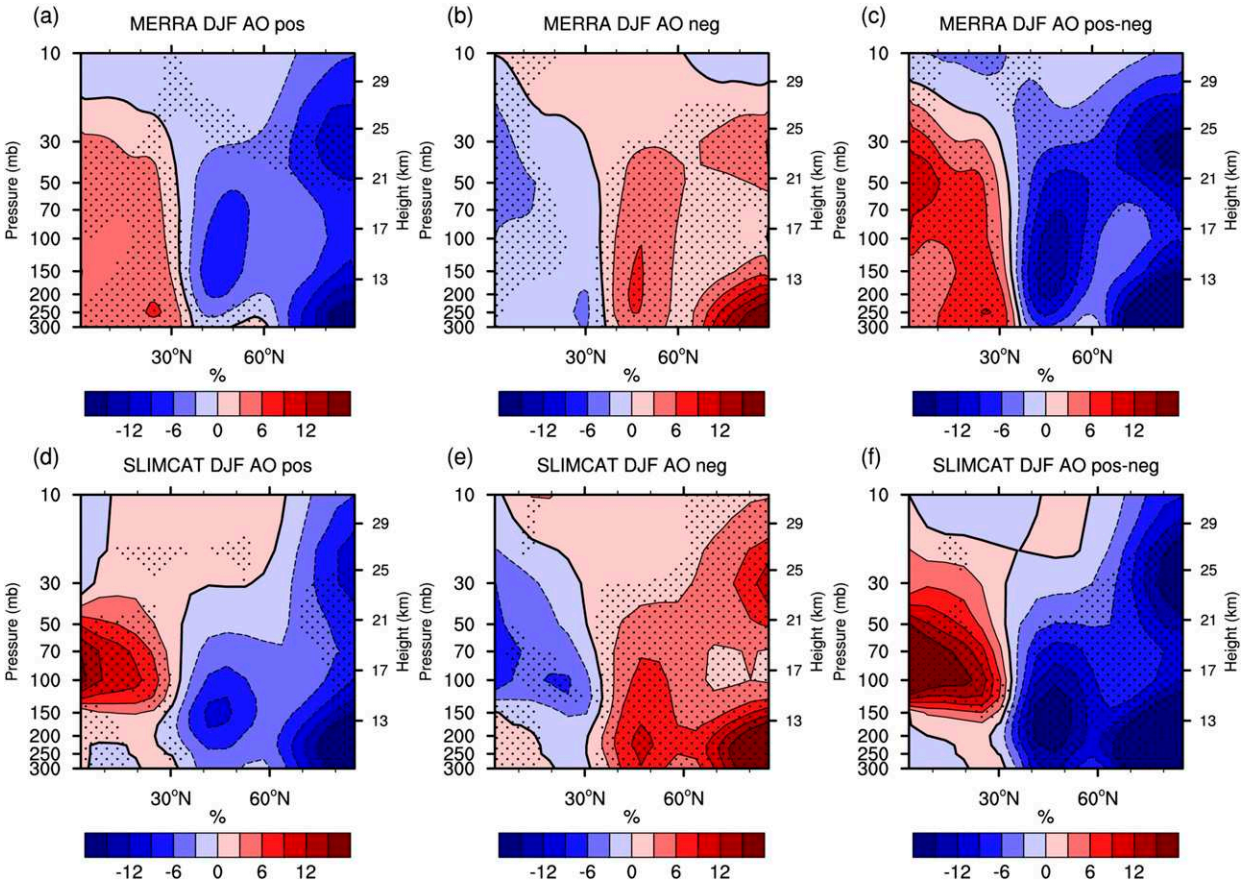

FIG. 3. Percentage anomaly in zonal-mean ozone over the Northern Hemisphere from (top) MERRA-2 data and (bottom) SLIMCAT simulation for (a),(d) positive and (b),(e) negative winter AO phases. (c),(f) Difference between the positive and negative percentage anomalies. The composited differences over the dotted regions are statistically significant at the 90% confidence level according to the Student's *t* test.

related to the cooler temperature between 30 and 200 hPa during the positive AO phase than the negative AO phase (Fig. 5b). There is also a chemical ozone loss centered between 30 and 70 hPa within 0°–30°N, which might be related to the heterogeneous chemistry caused by the Mount Pinatubo volcanic aerosols (Hofmann and Oltmans 1993; Solomon et al. 1996) during the years 1991 and 1992 used for composite analysis. In short, Figs. 5a and 5c illustrate that the chemical processes associated with AO phases deplete the Arctic lower stratospheric (50–150 hPa, 70°–90°N) chemical ozone by heterogeneous chemistry, but they increase the Arctic middle stratospheric (30–70 hPa, 70°–90°N) chemical ozone through gas-phase chemistry.

The above analysis reveals that the pattern of dynamical ozone anomalies is quite similar to the pattern of total ozone anomalies associated with AO events (Figs. 3c,f and 4a), suggesting that dynamical processes make the dominant contribution to AO-related ozone variability. A question arises as to which dynamical processes are responsible for this behavior in the Northern Hemisphere. Transport processes in general have a significant impact on the stratospheric ozone distribution; therefore, we further examine the transport of zonal-mean dynamical ozone via BDC advection and by eddies during anomalous AO events.

In Fig. 6, the dynamical ozone signal is decomposed into changes caused by the weakened meridional and vertical BDC transport, and eddy transport via mesoscale and other small-scale processes. Meridional BDC transport causes a depletion of ozone between 70 and 30 hPa in the Arctic (Fig. 6a), via reduced transport from the ozone-rich midlatitude region to the ozone-poor Arctic, corresponding to the reduction of dynamical ozone anomaly seen previously at this altitude (Fig. 4a). This negative meridional dynamical ozone transport implies weakening of the BDC during the positive phase of the AO, compared to the negative phase. The weakening of BDC is seen from the analysis of residual streamfunction. Figure 7 shows the composited

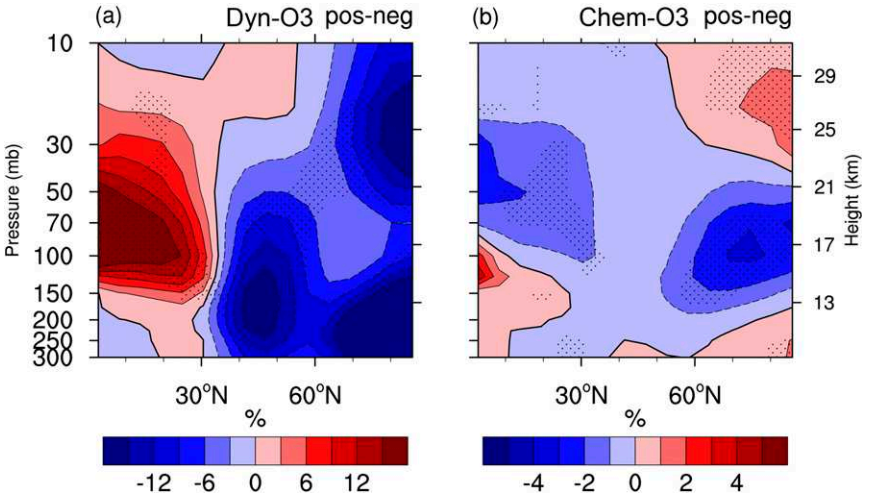

FIG. 4. Difference between positive-AO and negative-AO ozone percentage anomalies produced by (a) dynamical processes and (b) chemical processes. Data are from the SLIMCAT simulations. The composited differences over the dotted regions are statistically significant at the 90% confidence level according to the Student's *t* test.

anomalies of residual circulation streamfunction associated with positive and negative AO phases and their differences. According to Birner and Bönisch (2011), the residual streamfunction is computed as follows:

$$\overline{\chi}^*(p,\phi) = \int_0^p \frac{-2\pi R\cos\phi\overline{v}^*(p',\phi)}{g}dp', \qquad (4)$$

where $\overline{\chi}^*$ represents the residual streamfunction, $\overline{v}^*$ denotes the meridional velocity of BDC, p and ϕ denote pressure level and latitude, respectively, R is Earth's radius, and g represents the gravitational acceleration. Note that the residual streamfunction shows negative anomalies associated with positive AO phases, while there are positive anomalies for negative AO phases, suggesting that the residual streamfunction is weaker during positive AO phases than during negative AO phases. Accordingly, the BDC is weakened associated with positive AO events. The weakening of the BDC also leads to weakened downward vertical ozone transport in the Arctic stratosphere, resulting in a decrease in dynamical ozone transport from 30 to 250 hPa (Fig. 6b).

A dipole-like structure in the eddy transport ozone anomalies is found in the subtropics (Fig. 6c), with

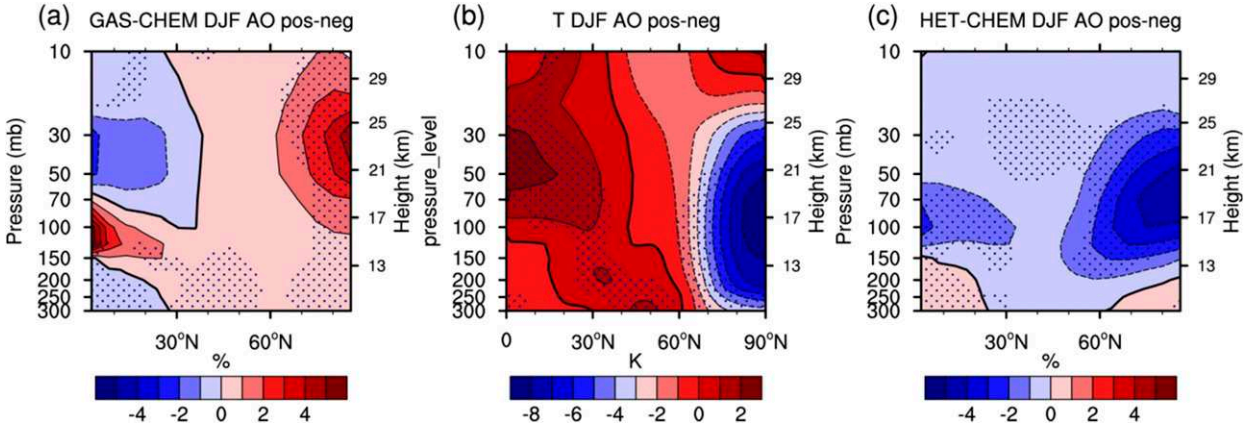

FIG. 5. (a) Difference of ozone percentage anomalies in the SLIMCAT experiment without heterogeneous chemistry between positive and negative AO phases. (b) Temperature difference between positive and negative AO phases. (c) Difference of AO-related ozone percentage anomalies (positive AO minus negative AO) between the SLIMCAT experiment with heterogeneous chemistry and the experiment without heterogeneous chemistry. The composited differences over the dotted regions are statistically significant at the 90% confidence level according to the Student's *t* test.

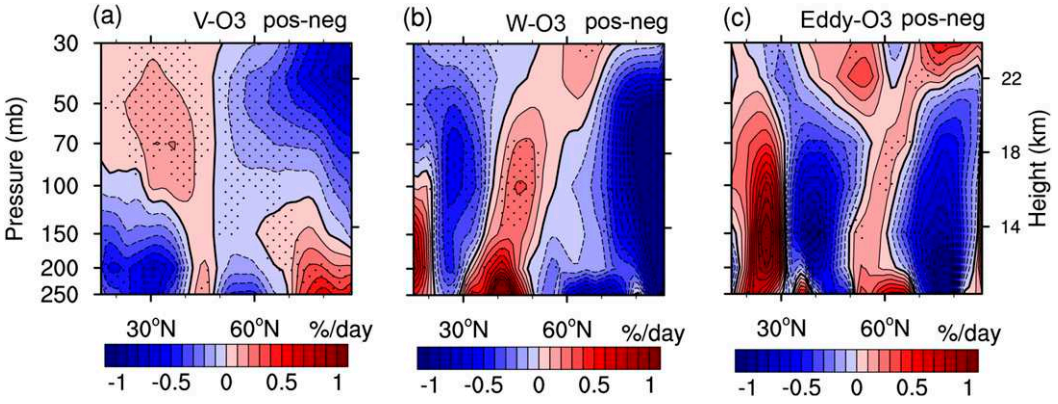

FIG. 6. Difference between positive-AO and negative-AO dynamically produced ozone percentage anomalies, decomposed into (a) meridional and (b) vertical BDC transport and (c) eddy transport rates, using MERRA-2 data. The composited differences over the dotted regions are statistically significant at the 90% confidence level according to the Student's *t* test.

positive (negative) ozone anomalies equatorward (poleward) of 30°N. Abalos et al. (2013) also found that eddy transport tends to increase ozone concentrations on the upper equatorward flank of the subtropical jet and decrease ozone poleward of 30°N, in a climatological sense. The dipole-like ozone differences between the positive and negative AO phases suggest that eddy transport is enhanced around the subtropical jet, leading to stronger ozone exchange between the midlatitudes (30°–50°N) and lower latitudes (15°–30°N). Thus, ozone concentration decreases in the midlatitude UTLS region, while ozone between 30 and 150 hPa in the tropics shows positive anomalies (Fig. 4a). In addition, eddy transport shows a negative anomaly in the Arctic at 50–250 hPa (Fig. 6c), suggesting that less ozone is transported from the midlatitudes (60°N) to the Arctic (70°–90°N) during positive AO phases than during negative AO phases, consistent with a strengthening of the polar jet and weakened mixing between mid-to-high latitudes and the Arctic during the positive AO phase. This process contributes to the dynamical ozone depletion seen in the Arctic UTLS (Fig. 4a).

The patterns of the decomposed dynamical ozone anomalies in the SLIMCAT simulations (Fig. 8), driven by the ERA-Interim data, are similar to those from MERRA-2 data (Fig. 6). However, the ozone anomalies from the SLIMCAT model are larger than those in MERRA-2 data, which may be a result of the coarser resolution of the SLIMCAT model grid used here. This is also consistent with the larger overall ozone anomalies seen in the SLIMCAT simulations compared to MERRA-2 (cf. Figs. 3a–c and 3d–f).

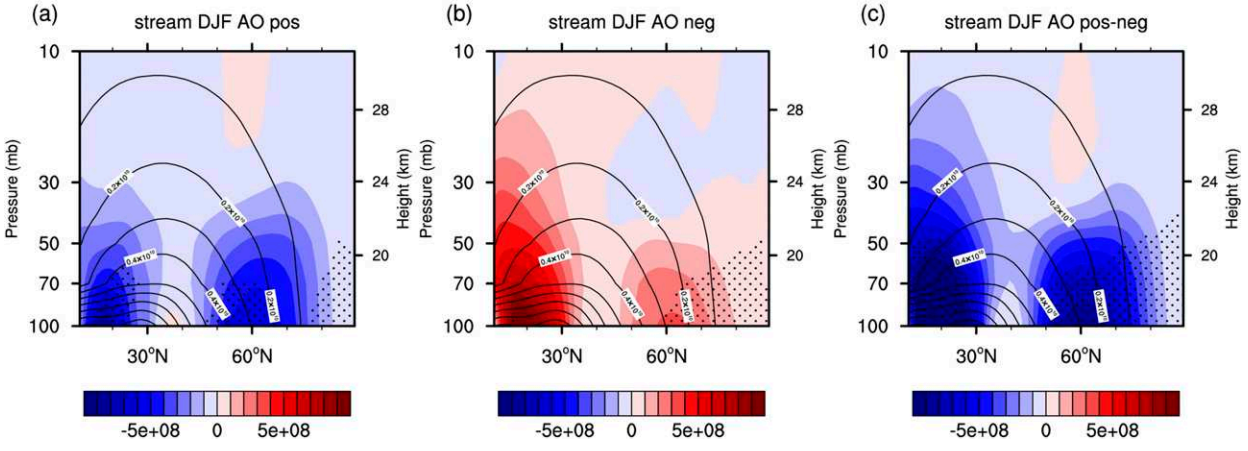

FIG. 7. Composite zonal-mean anomalies of residual streamfunction (shading; kg s^{-1}) over the Northern Hemisphere for (a) positive and (b) negative AO phases from MERRA-2 data. (c) Difference between the positive and negative anomalies. The contour lines represent the climatological mean of wintertime residual streamfunction for the period 1979–2012 (contour interval: 0.1 × 10 kg s^{-1}). The composited differences over the dotted regions are statistically significant at the 90% confidence level according to the Student's *t* test.

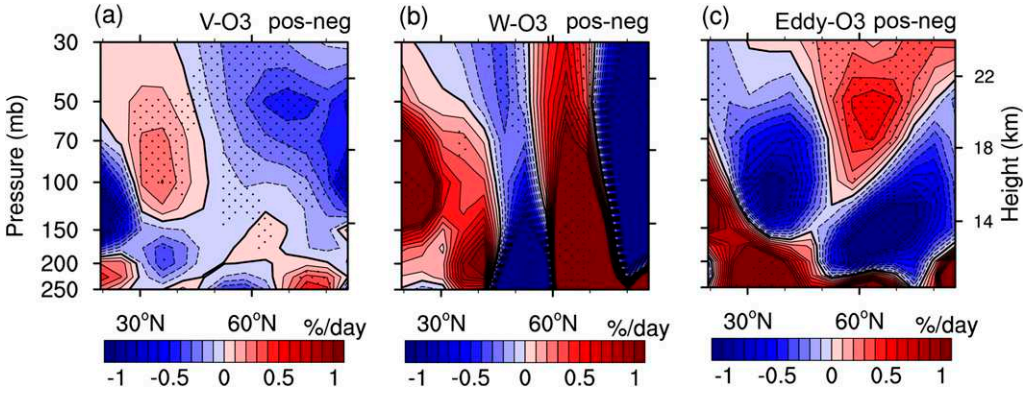

FIG. 8. As in Fig. 6, but for the SLIMCAT simulation data.

Figure 9 shows composites of the Rossby wave breaking (RWB) frequency, which is a good indicator of synoptic-scale and mesoscale mixing processes (Hitchman and Huesmann 2007; J. Zhang et al. 2015a), during the positive and negative AO phases. Positive AO events cause positive anomalies in RWB frequency around the subtropical jet at 30°N, while the RWB frequency near the polar jet around 60°N exhibits negative anomalies (Fig. 9a), suggesting that synoptic-scale mixing processes in the subtropics (subpolar regions) are enhanced (weakened). This makes sense, because the weakened subtropical jet during positive AO phases favors the transport of air from the midlatitudes (30°–50°N) to lower latitudes (15°–30°N), increasing ozone concentrations between 50 and 150 hPa in the tropics (Fig. 5a). In addition, stronger mixing around 30°N might also lead to increased transport of ozone-poor air from the lower latitudes (15°–30°N) to midlatitudes (30°–50°N). On the other hand, the enhanced polar jet acts as a barrier to weaken mixing between mid-to-high latitudes and the Arctic, reducing transport of ozone-rich air from the midlatitudes (50°–60°N) to the Arctic (70°–90°N). This result is consistent with the analysis of eddy transport anomalies shown previously (Figs. 6c and 8c). The anomalies in RWB frequency occurring during negative AO events are of opposite sign to those present during positive AO events (Fig. 9b). The differences in RWB frequency between the positive and negative AO phases further highlight the differences in synoptic-scale mixing processes that are present during the two AO phases.

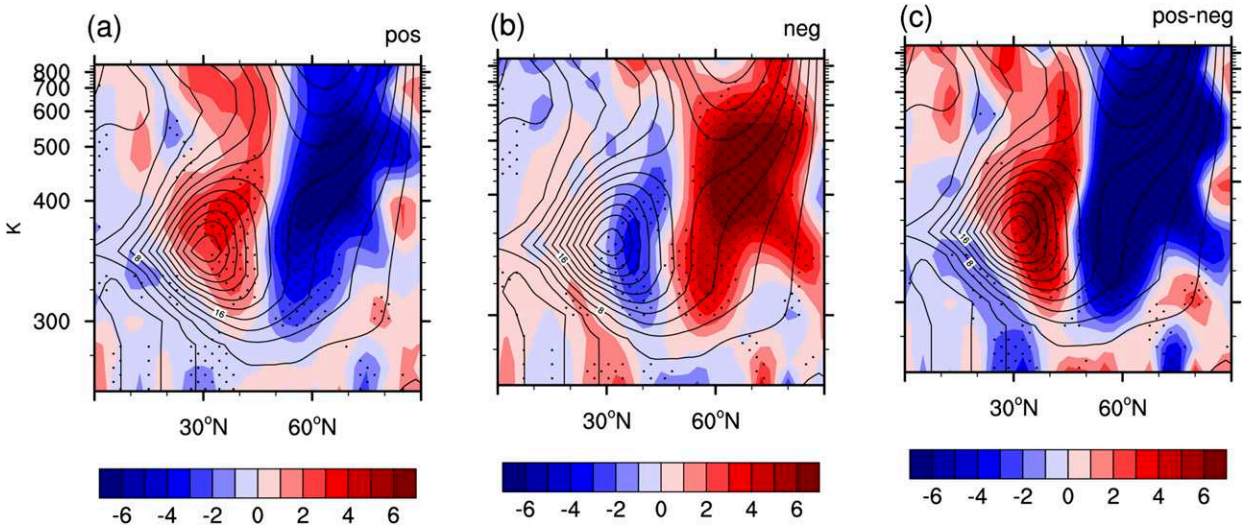

FIG. 9. Composite zonal-mean RWB frequency anomalies (shading; days) over the Northern Hemisphere for (a) positive and (b) negative AO phases, plotted against latitude and potential temperature (isentropic levels), from MERRA-2 data. (c) Difference between the positive and negative anomalies. RWB frequency is defined as the number of reversal days with negative meridional potential vorticity gradient per 100 days, following Hitchman and Huesmann (2007). The contour lines represent the climatological mean of wintertime RWB frequency for the period 1979–2012 (contour interval: 4 days). The composited differences over the dotted regions are statistically significant at the 90% confidence level according to the Student's *t* test.

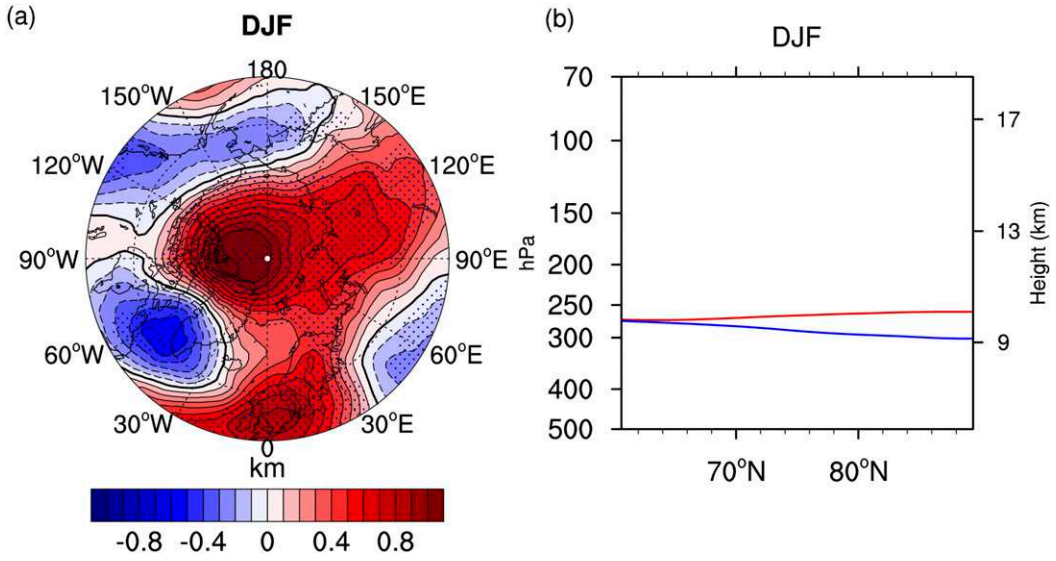

FIG. 10. (a) Difference between positive-AO and negative-AO composite thermal tropopause height anomalies from MERRA-2 data. (b) Red (blue) line shows the tropopause height in the positive (negative) phase of the AO. The composited differences in (a) over the dotted regions are statistically significant at the 90% confidence level according to the Student's *t* test.

Apart from the influence of dynamical transport, variations in tropopause height can also significantly affect the ozone distribution, especially in the UTLS region. Figure 10a presents the differences in thermal tropopause height between the positive and negative AO phases over the Arctic. There are positive anomalies in tropopause height over the Arctic, meaning that the Arctic tropopause is higher during positive AO events than during negative events. In contrast, the tropopause height over the Atlantic Ocean shows negative anomalies, implying a lower tropopause during the positive phase of the AO. The positive and negative centers of anomalous tropopause height resemble the NAO pattern, a fact that was also noted by Ambaum and Hoskins (2002). Figure 10b shows the changes in tropopause height associated with anomalous AO events. Previous studies showed that the raising of the tropopause can produce an overall upward shift in the ozone profile and thereby reduce ozone column density (Tung and Yang 1988; Tian et al. 2008). Tung and Yang (1988) proposed that the relationship between ozone column changes and shift in ozone profile is $\Delta\Omega/\Omega \cong \Delta z/H$, where Ω is ozone column density, $\Delta\Omega$ and Δz is change of ozone column density and tropopause height, respectively, and H denotes Arctic scale height (~8 km; Traub et al. 1995). We estimate that the Arctic tropopause averaged between 70° and 90°N rose by approximately 0.8 km in winter because of AO variability (see the red and blue lines in Fig. 10b), which leads to a 10% decrease in the ozone column in the Arctic during positive AO phases compared to negative AO phases.

5. Summary and conclusions

Using several observational datasets and an offline chemical transport model (SLIMCAT), this study has investigated the influence of AO variability on the distribution of ozone between 300 and 10 hPa over the Northern Hemisphere in winter, and the underlying mechanisms behind this influence. During the positive phase of the AO, stratospheric ozone concentrations are increased above the climatological mean in the lower latitudes (0°–30°N), while ozone poleward of 30°N is relatively depleted, creating a dipole pattern between the tropical and extratropical stratosphere. Negative AO events have the opposite effect on ozone. Of particular interest is the fact that, taking the difference between positive and negative AO phases, there are three centers of anomalously negative ozone concentrations in the extratropical stratosphere: in the Arctic middle stratosphere (30 hPa, 70°–90°N), Arctic UTLS (150–300 hPa, 70°–90°N), and midlatitude UTLS (70–300 hPa, 30°–60°N). The strongest negative correlations occur in the midlatitude UTLS, where correlation coefficients can reach approximately −0.6, while the largest variations in ozone forced by AO variability are found in the Arctic UTLS, because of large ozone variations in high latitudes. Differences in percentage ozone anomalies between the positive and negative AO phases in the Arctic UTLS can

exceed −30% in winter. Similar vertical patterns of ozone anomalies associated with AO variability are seen in reanalysis data, satellite data, and model simulations.

Ozone variations over the Northern Hemisphere that are associated with the AO can be mainly attributed to dynamical processes related to AO variability. The contribution of chemical processes to this variability is important in the Arctic, where ozone depletions of approximately 20% around 50–150 hPa poleward of 60°N can be attributed to AO-related chemistry anomalies.

Our analysis further reveals that during positive AO events, positive ozone anomalies between 50 and 150 hPa within 0°–30°N are related to the weakened meridional BDC transport and enhanced eddy transport; dynamical ozone depletion in the Arctic middle stratosphere during the positive AO phase is also caused by the weakening of the BDC. Consequently, less ozone is transported from the Arctic middle stratosphere to the Arctic lower stratosphere, leading to decreases in ozone in the Arctic UTLS region. Furthermore, the upward shift of the ozone vertical profile that is associated with a higher tropopause level and the weaker ozone transport from the midlatitudes (60°N) to the Arctic (70°–90°N) amplify the dynamical ozone depletions in the Arctic UTLS during positive AO events. Enhanced eddy ozone transport from the midlatitudes (30°–50°N) to the lower latitudes (15°–30°N) is responsible for the dynamical ozone decrease in the midlatitude UTLS during the positive AO phase. An increase in RWB frequency near the subtropical jet supports the notion that mixing between the midlatitude UTLS and lower latitudes is stronger during positive AO events. However, RWB frequency is reduced near the polar jet, suggesting that the ozone depletion associated with the strengthening of the polar vortex during the positive AO phase makes only a minor contribution to the ozone depletion in the midlatitude UTLS. Another interesting feature is that the positive ozone anomalies between 30 and 10 hPa in the Arctic, caused by reduced gas-phase chemistry rates due to the lower temperatures and lower ozone concentrations present during positive AO events compared with negative events, partially offset the dynamical ozone depletions at this altitude.

It is interesting to note that there is a positive correlation between AO and ozone around the region at 60°N from 100 to 70 hPa based on the MERRA-2 dataset (Fig. 1a); however, this positive correlation is very weak and even negative in the SLIMCAT data (Fig. 1d). This positive signal is absent in MLS and SBUV data due to insufficient data in this region (Figs. 1b–c). The positive correlation between AO and ozone suggests that the ozone at 60°N between 100 and 70 hPa is increased associated with positive AO events, which may be related to the positive eddy term in this region (Fig. 6c). During positive AO phases, the polar jet is strengthened and less poor-ozone air in the Arctic is transported toward 60°N, leading to positive ozone anomalies in this region. The positive eddy term disappears in the SLIMCAT data (Fig. 8c), which may be related to a coarser horizontal resolution of SLIMCAT grid (5.625° latitude × 5.625° longitude) than that of MERRA-2 grid (1.25° latitude × 1.25° longitude). Detailed analysis of the discrepancy in the positive correlation from different datasets requires further in-depth research.

Although the present study has clarified the effect of AO on the stratospheric ozone during winter, the contribution of stratospheric ozone to middle and lower tropospheric ozone via stratosphere–troposphere exchange associated with anomalous AO events is still unclear. To solve this question, fine vertical and horizontal distributions of ozone data in the UTLS are required. The analysis results of the AO-related ozone variability in the UTLS presented in this study may help improve forecasting tropospheric ozone variations over Europe and North America during AO events, which is worthy of more investigation in the future.

Acknowledgments. Funding for this work was provided by the National Natural Science Foundation of China (41575038, 41575039, and 41405043) and the 973 Project of China (Grant 2014CB441202). The SLIMCAT modelling work was supported by the U.K. National Centre for Atmospheric Science (NCAS). We acknowledge the use of datasets from the NOAA/Climate Prediction Center, MERRA-2, SBUV, and MLS. The authors would also like to thank Stacey Frith for her help with providing SBUV ozone data. We are also grateful to Dr. Kai Zhang for his help with processing MLS ozone data. The AO index data source is available online at http://www.cpc.ncep.noaa.gov/products/precip/CWlink/daily_ao_index/monthly.ao.index.b50.current.ascii. The MLS data used here are obtained from MLS version 3.3 level-2 products (available online at http://disc.sci.gsfc.nasa.gov/Aura/data-holdings/MLS/ml2o3.002.shtml).

REFERENCES

Abalos, M., W. J. Randel, D. E. Kinnison, and E. Serrano, 2013: Quantifying tracer transport in the tropical lower stratosphere using WACCM. *Atmos. Chem. Phys.*, **13**, 10 591–10 607, doi:10.5194/acp-13-10591-2013.

Alexeev, V. A., I. Esau, I. V. Polyakov, S. J. Byam, and S. Sorokina, 2012: Vertical structure of recent Arctic warming from observed data and reanalysis products. *Climatic Change*, **111**, 215–239, doi:10.1007/s10584-011-0192-8.

Allen, R. J., S. C. Sherwood, J. R. Norris, and C. S. Zender, 2012: Recent Northern Hemisphere tropical expansion primarily driven by black carbon and tropospheric ozone. *Nature*, **485**, 350–354, doi:10.1038/nature11097.

Ambaum, M. H. P., and B. J. Hoskins, 2002: The NAO troposphere–stratosphere connection. *J. Climate*, **15**, 1969–1978, doi:10.1175/1520-0442(2002)015<1969:TNTSC>2.0.CO;2.

Andrews, D. G., J. R. Holton, and C. B. Leovy, 1987: *Middle Atmosphere Dynamics.* Elsevier, 489 pp.

Angell, J. K., and J. Korshover, 1973: Quasi-biennial and long-term fluctuations in total ozone. *Mon. Wea. Rev.*, **101**, 426–443, doi:10.1175/1520-0493(1973)101<0426:QALFIT>2.3.CO;2.

Appenzeller, C., A. K. Weiss, and J. Staehelin, 2000: North Atlantic Oscillation modulates total ozone winter trends. *Geophys. Res. Lett.*, **27**, 1131–1134, doi:10.1029/1999GL010854.

Austin, J., and R. J. Wilson, 2006: Ensemble simulations of the decline and recovery of stratospheric ozone. *J. Geophys. Res.*, **111**, D16314, doi:10.1029/2005JD006907.

——, and Coauthors, 2010: Decline and recovery of total column ozone using a multimodel time series analysis. *J. Geophys. Res.*, **115**, D00M10, doi:10.1029/2010JD013857.

Baldwin, M. P., and T. J. Dunkerton, 2001: Stratospheric harbingers of anomalous weather regimes. *Science*, **294**, 581–584, doi:10.1126/science.1063315.

Bhartia, P., and Coauthors, 2013: Solar backscatter UV (SBUV) total ozone and profile algorithm. *Atmos. Meas. Tech.*, **6**, 2533–2548, doi:10.5194/amt-6-2533-2013.

Birner, T., and H. Bönisch, 2011: Residual circulation trajectories and transit times into the extratropical lowermost stratosphere. *Atmos. Chem. Phys.*, **11**, 817–827, doi:10.5194/acp-11-817-2011.

Bosilovich, M. G., and Coauthors, 2015: MERRA-2: Initial evaluation of the climate. NASA Tech. Memo. NASA/TM-2015-104606/Vol. 43, 145 pp. [Available online at http://gmao.gsfc.nasa.gov/reanalysis/MERRA-2/docs/.]

Bowman, K. P., 1989: Global patterns of the quasi-biennial oscillation in total ozone. *J. Atmos. Sci.*, **46**, 3328–3343, doi:10.1175/1520-0469(1989)046<3328:GPOTQB>2.0.CO;2.

Cagnazzo, C., and Coauthors, 2009: Northern winter stratospheric temperature and ozone responses to ENSO inferred from an ensemble of chemistry climate models. *Atmos. Chem. Phys.*, **9**, 8935–8948, doi:10.5194/acp-9-8935-2009.

Chandra, S., and R. D. McPeters, 1994: The solar cycle variation of ozone in the stratosphere inferred from *Nimbus 7* and *NOAA 11* satellites. *J. Geophys. Res.*, **99**, 20 665–20 671, doi:10.1029/94JD02010.

Chipperfield, M., 2006: New version of the TOMCAT/SLIMCAT off-line chemical transport model: Intercomparison of stratospheric tracer experiments. *Quart. J. Roy. Meteor. Soc.*, **132**, 1179–1203, doi:10.1256/qj.05.51.

Cohen, J. L., J. C. Furtado, M. A. Barlow, V. A. Alexeev, and J. E. Cherry, 2012: Arctic warming, increasing snow cover and widespread boreal winter cooling. *Environ. Res. Lett.*, **7**, 014007, doi:10.1088/1748-9326/7/1/014007.

——, and Coauthors, 2014: Recent Arctic amplification and extreme mid-latitude weather. *Nat. Geosci.*, **7**, 627–637, doi:10.1038/ngeo2234.

Creilson, J. K., J. Fishman, and A. E. Wozniak, 2005: Arctic Oscillation-induced variability in satellite-derived tropospheric ozone. *Geophys. Res. Lett.*, **32**, L14822, doi:10.1029/2005GL023016.

Dee, D. P., and Coauthors, 2011: The ERA-Interim reanalysis: Configuration and performance of the data assimilation system. *Quart. J. Roy. Meteor. Soc.*, **137**, 553–597, doi:10.1002/qj.828.

Degenstein, D. A., A. E. Bourassa, C. Z. Roth, and E. J. Llewellyn, 2009: Limb scatter ozone retrieval from 10 to 60 km using a multiplicative algebraic reconstruction technique. *Atmos. Chem. Phys.*, **9**, 6521–6529, doi:10.5194/acp-9-6521-2009.

Dhomse, S. S., S. M. Weber, I. Wohltmann, M. Rex, and J. P. Burrows, 2006: On the possible causes of recent increases in northern hemispheric total ozone from a statistical analysis of satellite data from 1979 to 2003. *Atmos. Chem. Phys.*, **6**, 1165–1180, doi:10.5194/acp-6-1165-2006.

——, M. P. Chipperfield, W. Feng, R. Hossaini, G. W. Mann, and M. L. Santee, 2015: Revisiting the hemispheric asymmetry in midlatitude ozone changes following the Mount Pinatubo eruption: A 3-D model study. *Geophys. Res. Lett.*, **42**, 3038–3047, doi:10.1002/2015GL063052.

Douglass, A. R., S. E. Strahan, L. D. Oman, and R. S. Stolarski, 2014: Understanding differences in chemistry climate model projections of stratospheric ozone. *J. Geophys. Res. Atmos.*, **119**, 4922–4939, doi:10.1002/2013JD021159.

Eyring, V., and Coauthors, 2010: Multi-model assessment of stratospheric ozone return dates and ozone recovery in CCMVal-2 models. *Atmos. Chem. Phys.*, **10**, 9451–9472, doi:10.5194/acp-10-9451-2010.

Feng, W., and Coauthors, 2005: Three-dimensional model study of the Antarctic ozone hole in 2002 and comparison with 2000. *J. Atmos. Sci.*, **62**, 822–837, doi:10.1175/JAS-3335.1.

——, M. P. Chipperfield, S. Davies, P. von der Gathen, E. Kyrö, C. M. Volk, A. Ulanovsky, and G. Belyaev, 2007: Large chemical ozone loss in 2004/2005 Arctic winter/spring. *Geophys. Res. Lett.*, **34**, L09803, doi:10.1029/2006GL029098.

——, and Coauthors, 2011: Modelling the effect of denitrification on polar ozone depletion for Arctic winter 2004/2005. *Atmos. Chem. Phys.*, **11**, 6559–6573, doi:10.5194/acp-11-6559-2011.

Frith, S., N. Kramarova, R. Stolarski, R. McPeters, P. Bhartia, and G. Labow, 2014: Recent changes in total column ozone based on the SBUV version 8.6 Merged Ozone Data Set. *J. Geophys. Res. Atmos.*, **119**, 9735–9751, doi:10.1002/2014JD021889.

Frossard, L., and Coauthors, 2013: On the relationship between total ozone and atmospheric dynamics and chemistry at mid-latitudes—Part 1: Statistical models and spatial fingerprints of atmospheric dynamics and chemistry. *Atmos. Chem. Phys.*, **13**, 147–164, doi:10.5194/acp-13-147-2013.

Fujiwara, M., K. Kita, and T. Ogawa, 1998: Stratosphere–troposphere exchange of ozone associated with the equatorial Kelvin wave as observed with ozonesondes and rawinsondes. *J. Geophys. Res.*, **103**, 19 173–19 182, doi:10.1029/98JD01419.

Hadjinicolaou, P., A. Jrrar, J. A. Pyle, and L. Bishop, 2002: The dynamically driven long-term trend in stratospheric ozone over northern middle latitudes. *Quart. J. Roy. Meteor. Soc.*, **128**, 1393–1412, doi:10.1002/qj.200212858301.

Hess, P. G., and J. F. Lamarque, 2007: Ozone source attribution and its modulation by the Arctic oscillation during the spring months. *J. Geophys. Res.*, **112**, D11303, doi:10.1029/2006JD007557.

Hitchman, M. H., and A. S. Huesmann, 2007: A seasonal climatology of Rossby wave breaking in the 320–2000-K layer. *J. Atmos. Sci.*, **64**, 1922–1940, doi:10.1175/JAS3927.1.

Hofmann, D. J., and S. J. Oltmans, 1993: Anomalous Antarctic ozone during 1992: Evidence for Pinatubo volcanic aerosol effects. *J. Geophys. Res.*, **98**, 18 555–18 561, doi:10.1029/93JD02092.

Holton, J. R., P. H. Haynes, M. E. McIntyre, A. R. Douglass, R. B. Rood, and L. Pfister, 1995: Stratosphere–troposphere exchange. *Rev. Geophys.*, **33**, 403–439, doi:10.1029/95RG02097.

Kerr, J. B., and C. T. McElroy, 1993: Evidence of large upward trends of ultraviolet-B radiation linked to ozone depletion. *Science*, **262**, 1032–1034, doi:10.1126/science.262.5136.1032.

Knudsen, B. M., and J. U. Grooss, 2000: Northern midlatitude stratospheric ozone dilution in spring modeled with simulated

mixing. *J. Geophys. Res.*, **105**, 6885–6890, doi:10.1029/1999JD901076.

Lamarque, J. F., and P. G. Hess, 2004: Arctic Oscillation modulation of the Northern Hemisphere spring tropospheric ozone. *Geophys. Res. Lett.*, **31**, L06127, doi:10.1029/2003GL019116.

Li, F., R. S. Stolarski, and P. A. Newman, 2009: Stratospheric ozone in the post-CFC era. *Atmos. Chem. Phys.*, **9**, 2207–2213, doi:10.5194/acp-9-2207-2009.

——, Y. V. Vikhliaev, P. A. Newman, S. Pawson, J. Perlwitz, D. W. Waugh, and A. R. Douglass, 2016: Impacts of interactive stratospheric chemistry on Antarctic and Southern Ocean climate change in the Goddard Earth Observing System, version 5 (GEOS-5). *J. Climate*, **29**, 3199–3218, doi:10.1175/JCLI-D-15-0572.1.

Li, K.-F., and K.-K. Tung, 2014: Quasi-biennial oscillation and solar cycle influences on winter Arctic total ozone. *J. Geophys. Res. Atmos.*, **119**, 5823–5835, doi:10.1002/2013JD021065.

——, B. Tian, D. E. Waliser, M. J. Schwartz, J. L. Neu, J. R. Worden, and Y. L. Yung, 2012: Vertical structure of MJO-related subtropical ozone variations from MLS, TES, and SHADOZ data. *Atmos. Chem. Phys.*, **12**, 425–436, doi:10.5194/acp-12-425-2012.

Lindsay, R., M. Wensnahan, A. Schweiger, and J. Zhang, 2014: Evaluation of seven different atmospheric reanalysis products in the Arctic. *J. Climate*, **27**, 2588–2606, doi:10.1175/JCLI-D-13-00014.1.

Liu, C., Y. Liu, Z. Cai, S. Gao, D. Lü, and E. Kyrölä, 2009: A Madden–Julian oscillation–triggered record ozone minimum over the Tibetan Plateau in December 2003 and its association with stratospheric "low-ozone pockets." *Geophys. Res. Lett.*, **36**, L15830, doi:10.1029/2009GL039025.

Liu, J. J., D. B. A. Jones, J. R. Worden, D. Noone, M. Parrington, and J. Kar, 2009: Analysis of the summertime buildup of tropospheric ozone abundances over the Middle East and North Africa as observed by the Tropospheric Emission Spectrometer instrument. *J. Geophys. Res.*, **114**, D05304, doi:10.1029/2008JD010993.

——, ——, S. Zhang, and J. Kar, 2011: Influence of interannual variations in transport on summertime abundances of ozone over the Middle East. *J. Geophys. Res.*, **116**, D20310, doi:10.1029/2011JD016188.

——, and Coauthors, 2013: A global ozone climatology from ozone soundings via trajectory mapping: A stratospheric perspective. *Atmos. Chem. Phys.*, **13**, 11 441–11 464, doi:10.5194/acp-13-11441-2013.

Livesey, N., and Coauthors, 2011: EOS MLS version 3.3 level 2 data quality and description document. Jet Propulsion Laboratory Tech. Rep. JPL D-33509, 162 pp.

Manney, G. L., and Coauthors, 2011: Unprecedented Arctic ozone loss in 2011. *Nature*, **478**, 469–475, doi:10.1038/nature10556.

McPeters, R. D., P. Bhartia, D. Haffner, G. J. Labow, and L. Flynn, 2013: The version 8.6 SBUV ozone data record: An overview. *J. Geophys. Res. Atmos.*, **118**, 8032–8039, doi:10.1002/jgrd.50597.

Monier, E., and B. C. Weare, 2011: Climatology and trends in the forcing of the stratospheric ozone transport. *Atmos. Chem. Phys.*, **11**, 6311–6323, doi:10.5194/acp-11-6311-2011.

Orsolini, Y., P. Simon, and D. Cariolle, 1995: Filamentation and layering of an idealized tracer by observed winds in the lower stratosphere. *Geophys. Res. Lett.*, **22**, 839–842, doi:10.1029/95GL00389.

Overland, J. E., and M. Wang, 2005: The Arctic climate paradox: The recent decrease of the Arctic Oscillation. *Geophys. Res. Lett.*, **32**, L06701, doi:10.1029/2004GL021752.

Prather, M. J., 1986: Numerical advection by conservation of second-order moments. *J. Geophys. Res.*, **91**, 6671–6681, doi:10.1029/JD091iD06p06671.

Randel, W. J., R. R. Garcia, N. Calvo, and D. Marsh, 2009: ENSO influence on zonal mean temperature and ozone in the tropical lower stratosphere. *Geophys. Res. Lett.*, **36**, L15822, doi:10.1029/2009GL039343.

Reinsel, G. C., A. J. Miller, E. C. Weatherhead, L. E. Flynn, R. M. Nagatani, G. C. Tiao, and D. J. Wuebbles, 2005: Trend analysis of total ozone data for turnaround and dynamical contributions. *J. Geophys. Res.*, **110**, D16306, doi:10.1029/2004JD004662.

Rieder, H. E., and Coauthors, 2013: On the relationship between total ozone and atmospheric dynamics and chemistry at mid-latitudes—Part 2: The effects of the El Niño/Southern Oscillation, volcanic eruptions and contributions of atmospheric dynamics and chemistry to long-term total ozone changes. *Atmos. Chem. Phys.*, **13**, 165–179, doi:10.5194/acp-13-165-2013.

——, L. M. Polvani, and S. Solomon, 2014: Distinguishing the impacts of ozone depleting substances and well-mixed greenhouse gases on Arctic stratospheric ozone and temperature trends. *Geophys. Res. Lett.*, **41**, 2652–2660, doi:10.1002/2014GL059367.

Rienecker, M. M., and Coauthors, 2011: MERRA: NASA's Modern-Era Retrospective Analysis for Research and Applications. *J. Climate*, **24**, 3624–3648, doi:10.1175/JCLI-D-11-00015.1.

Rozanov, E. V., M. E. Schlesinger, N. G. Andronova, F. Yang, S. L. Malyshev, V. A. Zubov, T. A. Egorova, and B. Li, 2002: Climate/chemistry effects of the Pinatubo volcanic eruption simulated by the UIUC stratosphere/troposphere GCM with interactive photochemistry. *J. Geophys. Res.*, **107**, 4594, doi:10.1029/2001JD000974.

——, M. Schraner, T. Egorova, A. Ohmura, M. Wild, W. Schmutz, and T. Peter, 2005: Solar signal in atmospheric ozone, temperature and dynamics simulated with CCM SOCOL in transient mode. *Mem. Soc. Astron. Ital.*, **76**, 876–879.

Schnadt, C., and M. Dameris, 2003: Relationship between North Atlantic Oscillation changes and stratospheric ozone recovery in the Northern Hemisphere in a chemistry–climate model. *Geophys. Res. Lett.*, **30**, 1487, doi:10.1029/2003GL017006.

Sioris, C. E., C. A. McLinden, V. E. Fioletov, C. Adams, J. M. Zawodny, A. E. Bourassa, C. Z. Roth, and D. A. Degenstein, 2014: Trend and variability in ozone in the tropical lower stratosphere over 2.5 solar cycles observed by SAGE II and OSIRIS. *Atmos. Chem. Phys.*, **14**, 3479–3496, doi:10.5194/acpd-13-16661-2013.

Solomon, S., R. Garcia, and F. Stordal, 1985: Transport processes and ozone perturbations. *J. Geophys. Res.*, **90**, 12 981–12 989, doi:10.1029/JD090iD07p12981.

——, R. W. Portmann, R. R. Garcia, L. W. Thomason, L. R. Poole, and M. P. McCormick, 1996: The role of aerosol variations in anthropogenic ozone depletion at northern midlatitudes. *J. Geophys. Res.*, **101**, 6713–6727, doi:10.1029/95JD03353.

Steinbrecht, W., U. Köhler, H. Claude, M. Weber, J. P. Burrows, and R. J. van der A, 2011: Very high ozone columns at northern mid-latitudes in 2010. *Geophys. Res. Lett.*, **38**, L06803, doi:10.1029/2010GL046634.

Thompson, D. W. J., and J. M. Wallace, 2000: Annular modes in the extratropical circulation. Part I: Month-to-month variability. *J. Climate*, **13**, 1000–1016, doi:10.1175/1520-0442(2000)013<1000:AMITEC>2.0.CO;2.

——, and ——, 2001: Regional climate impacts of the Northern Hemisphere annular mode. *Science*, **293**, 85–89, doi:10.1126/science.1058958.

——, S. Solomon, P. J. Kushner, M. H. England, K. M. Grise, and D. J. Karoly, 2011: Signatures of the Antarctic ozone hole in Southern Hemisphere surface climate change. *Nat. Geosci.*, **4**, 741–749, doi:10.1038/ngeo1296.

Tian, B. J., Y. L. Yung, D. E. Waliser, T. Tyranowski, L. Kuai, E. J. Fetzer, and F. W. Irion, 2007: Intraseasonal variations of the tropical total ozone and their connection to the Madden–Julian oscillation. *Geophys. Res. Lett.*, **34**, L08704, doi:10.1029/2007GL029451.

Tian, W., and M. P. Chipperfield, 2005: A new coupled chemistry–climate model for the stratosphere: The importance of coupling for future O_3-climate predictions. *Quart. J. Roy. Meteor. Soc.*, **131**, 281–303, doi:10.1256/qj.04.05.

——, ——, and Q. Huang, 2008: Effects of the Tibetan Plateau on total column ozone distribution. *Tellus*, **60B**, 622–635, doi:10.1111/j.1600-0889.2008.00338.x.

Traub, W. A., K. W. Jucks, D. G. Johnson, and K. V. Chance, 1995: Subsidence of the Arctic stratosphere determined from thermal emission of hydrogen fluoride. *J. Geophys. Res.*, **100**, 11 261–11 267, doi:10.1029/95JD00619.

Tung, K. K., and H. Yang, 1988: Dynamic variability of column ozone. *J. Geophys. Res.*, **93**, 11 123–11 128, doi:10.1029/JD093iD09p11123.

——, and ——, 1994: Global QBO in circulation and ozone. Part II: A simple mechanistic model. *J. Atmos. Sci.*, **51**, 2708–2721, doi:10.1175/1520-0469(1994)051<2708:GQICAO>2.0.CO;2.

Weare, B. C., 2010: Madden–Julian oscillation in the tropical stratosphere. *J. Geophys. Res.*, **115**, D17113, doi:10.1029/2009JD013748.

Weiss, A. K., J. Staehelin, C. Appenzeller, and N. R. P. Harris, 2001: Chemical and dynamical contributions to ozone profile trends of the Payerne (Switzerland) balloon soundings. *J. Geophys. Res.*, **106**, 22 685–22 694, doi:10.1029/2000JD000106.

WMO, 2007: Scientific assessment of ozone depletion: 2006. World Meteorological Organization/United Nations Environment Programme Rep. 50, 572 pp.

——, 2011: Scientific assessment of ozone depletion: 2010. World Meteorological Organization/United Nations Environment Programme Rep. 52, 516 pp.

Xie, F., J. Li, W. Tian, J. Zhang, and J. Shu, 2014a: The impacts of two types of El Niño on global ozone variations in the last three decades. *Adv. Atmos. Sci.*, **31**, 1113–1126, doi:10.1007/s00376-013-3166-0.

——, ——, ——, ——, and C. Sun, 2014b: The relative impacts of El Niño Modoki, canonical El Niño, and QBO on tropical ozone changes since the 1980s. *Environ. Res. Lett.*, **9**, 064020, doi:10.1088/1748-9326/9/6/064020.

——, and Coauthors, 2016: A connection from Arctic stratospheric ozone to El Niño–Southern Oscillation. *Environ. Res. Lett.*, **11**, 124026, doi:10.1088/1748-9326/11/12/124026.

Zhang, J., W. Tian, F. Xie, H. Tian, J. Luo, J. Zhang, W. Liu, and S. Dhomse, 2014: Climate warming and decreasing total column ozone over the Tibetan Plateau during winter and spring. *Tellus*, **66B**, 23415, http://dx.doi.org/10.3402/tellusb.v66.23415.

——, ——, Z. Wang, F. Xie, and F. Wang, 2015a: The influence of ENSO on northern midlatitude ozone during the winter to spring transition. *J. Climate*, **28**, 4774–4793, doi:10.1175/JCLI-D-14-00615.1.

——, ——, F. Xie, Y. Li, F. Wang, J. Huang, and H. Tian, 2015b: Influence of the El Niño Southern Oscillation on the total ozone column and clear-sky ultraviolet radiation over China. *Atmos. Environ.*, **120**, 205–216, doi:10.1016/j.atmosenv.2015.08.080.

——, ——, M. P. Chipperfield, F. Xie, and J. Huang, 2016: Persistent shift of the Arctic polar vortex towards the Eurasian continent in recent decades. *Nat. Climate Change*, **6**, 1094–1099, doi:10.1038/nclimate3136.

Zhang, Y. L., Y. Liu, C. X. Liu, and V. F. Sofieva, 2015: Satellite measurements of the Madden–Julian oscillation in wintertime stratospheric ozone over the Tibetan Plateau and East Asia. *Adv. Atmos. Sci.*, **32**, 1481–1492, doi:10.1007/s00376-015-5005-y.

Ziemke, J. R., and S. Chandra, 1999: Seasonal and interannual variabilities in tropical tropospheric ozone. *J. Geophys. Res.*, **104**, 21 425–21 442, doi:10.1029/1999JD900277.